


Article

Modelling of Flow Parameters through Subsurface Drainage Modules for Application in BIOECODS

Abdurrasheed Sa'id Abdurrasheed ^{1,2,*} , Khamaruzaman Wan Yusof ¹,
Ebrahim Hamid Hussein Alqadami ¹, Husna Takaijudin ¹, Aminuddin Ab. Ghani ³,
Muhammad Mujahid Muhammad ⁴, Abdulkadir Taofeeq Sholagberu ⁵,
Muhammad Kashfy Zainalfikry ³, Manal Osman ¹ and Mohammed Shihab Patel ¹

¹ Department of Civil and Environmental Engineering, Universiti Teknologi PETRONAS, Bandar Seri Iskandar 32610, Perak, Malaysia

² Department of Civil Engineering, Ahmadu Bello University, Zaria 810107, Nigeria

³ River Engineering and Urban Drainage Research Centre (REDAC), Engineering Campus, Universiti Sains Malaysia, Nibong Tebal 14300, Pulau Pinang, Malaysia

⁴ Department of Water Resources and Environmental Engineering, Ahmadu Bello University, Zaria 810107, Nigeria

⁵ Department of Water Resources and Environmental Engineering, University of Ilorin, Ilorin 240103, Nigeria

* Correspondence: asa00@ymail.com (A.S.A.); khamaruzaman.yusof@utp.edu.my (K.W.Y.);
Tel.: +60-115-1919-747 (A.S.A.)

Received: 15 June 2019; Accepted: 24 July 2019; Published: 31 August 2019



Abstract: The flow resistance of the existing modules in the bio-ecological drainage system (BIOECODS) is high and may lead to flood instead of its mitigation. As part of efforts to enhance the performance of the system, the river engineering and urban drainage research center (REDAC) module was developed. This study modelled the hydrodynamics of flow through this module using FLOW-3D and laboratory experiments for two cases of free flow without module (FFWM) and flow with a module (FWM) to understand and visualize the effects of the module. With less than 5% error between the numerical and experimental results, REDAC module altered the flow pattern and created resistance by increasing the Manning's roughness coefficient at the upstream, depth-averaged flow velocity (43.50 cm/s to about 46.50 cm/s) at the downstream and decreasing water depth (7.75–6.50 cm). These variations can be attributed to the complex nature of the module pattern with further increase across the porous openings. Therefore, the technique used herein can be applied to characterize the behavior of fluids in larger arrangements of modules and under different flow conditions without the need for expensive laboratory experiments.

Keywords: hydrodynamics; FLOW-3D; bioecods; redac; flow resistance; subsurface drainage; module; attenuation

1. Introduction

Urbanization sometimes comes with lots of changes in natural hydrology as a result of more impervious surfaces such as pavements and rooftops [1,2]. Flood peaks, water pollution, scouring of channels and sedimentation had been highlighted by Ainan et al. [3] and Barber et al. [4] as the potential consequences of this phase of development. This necessitates the development of new sustainable stormwater management and control strategies that utilize the concept of “control at source” as highlighted by Fletcher et al. [5] and can promote infiltration, reuse, quality, and quantity enhancement [3,6]. The river engineering and urban drainage research center (REDAC) through department of irrigation and drainage (DID) Malaysia has developed a system called the bioecological drainage system (BIOECODS) that utilizes subsurface modules or storage tanks (Figure 1), dry and

wet ponds as well as constructed grass swales to promote groundwater recharge, reuse, quality and quantity control [7–9]. The subsurface drainage modules are designed in different shape and patterns to increase lag time in the flow (attenuation), reduce the volume by enhancing groundwater recharge and promote storage [1]. As part of efforts to enhance the performance of this technology, the REDAC module was developed. This is a new type of module as shown in Figure 1 with the (*Bunga Cengkih*) pattern designed based on the fact that the flow resistance of the existing module in the BIOECODS is high resulting in low-flow velocity and high attenuation which if not properly handled may lead to flooding instead of mitigating it. However, hydraulic performance in terms of flow resistance as well as the flow pattern of this type of module is still not fully understood.

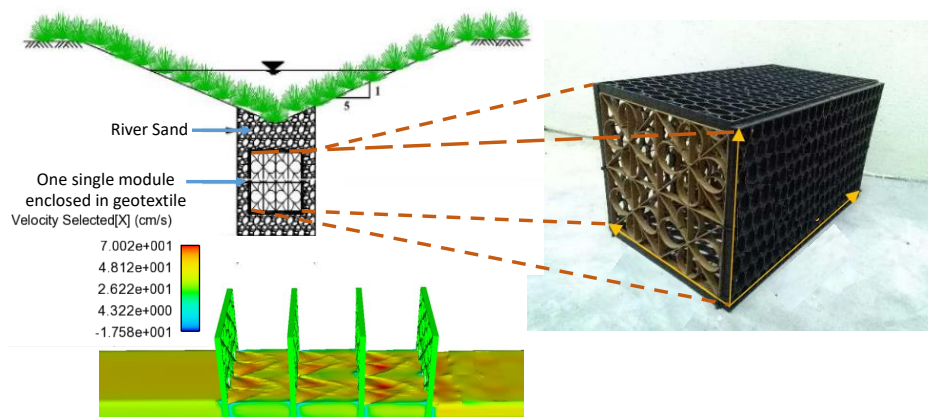


Figure 1. Redac module in bioswale [1].

Different methods have been applied to study the hydraulic behavior of modules in channels including field measurements by Ahmad et al. [10], and Lai et al. [11], analytical and laboratory experiments as well as numerical techniques [12,13]. However, very few methods are able to explain, in detail, the physics between fluid flow and solid structure interactions that result in high-flow resistance leading to very low-flow velocity as well as energy dissipation in the subsurface modules. For example, experimental studies were conducted to determine the impact of the module on flow pattern by Kee et al. [14], Manning's roughness coefficient by Zakaria [13], Muhammad et al. [15] and Pradhan et al. [16], quality and quantity control and most recently effects of backwater on the hydraulic performance of the module [2]. In terms of numerical methods, Sánchez et al. [17] applied computational fluid dynamics (CFD) to characterize the hydraulic performance of a drainage network and develop a clear validation with experimental data. Faram et al. [18] also carried out similar studies with CFD by introducing tracer elements. Details about the application of CFD in urban drainage can be found in [19].

In principle, real-world flow problems are too complex to be addressed solely by theory or experimentation [20]. A lot of limitations had been identified in physical modelling and recent advancements in numerical methods in solving complex fluid-structure interactions increase its adoption rate [21,22]. In view of the continuous advances in numerical techniques, this study adopts a general purpose CFD software known as FLOW-3D because of its robustness, tendency to numerically reproduce flow and turbulent conditions with clear visualization power at different stages. Additionally, it has special capabilities for accurately studying free-surface flows and giving valuable insight into many physical flow processes. It differs from other CFD software specifically in its treatment of flowing fluid surfaces. The program uses special numerical methods to track the location of surfaces and to apply the proper dynamic boundary conditions at those surfaces [23,24]. Also, FLOW-3D had been widely used to interpret and validate laboratory and field experiments as well as provide other benefits such as shortening research periods, lower costs and effective repeatability [25]. CFD techniques had been applied in urban drainage systems [17,26].

This paper, therefore, modelled the hydrodynamics of flow through the REDAC module using a numerical technique and validated it with laboratory experimental data.

2. Theory and Governing Equations

FLOW-3D is a general purpose and widely used commercial CFD code capable of modelling unsteady flows through complex geometries in multidimensional forms. It was originally described by Hirt [23] and developed by FlowScience, Inc. [27]. FLOW-3D utilizes the volume of fluid (VOF) concept which defines fluid fraction in a fluid domain using fluid volume function V_F (F). When $V_F = 0$, the domain is considered empty without fluid, when $V_F = 1$, it is considered filled with fluid and in the case of a free water surface V_F has a value between 0 and 1 as shown in Figure 2 [25]. A total of six different turbulence models including Prandtl mixing length model, large eddy simulation (LES) model, the one equation, re-normalization group (RNG), $k-\epsilon$ and $k-\omega$ models are available in FLOW-3D. Equations governing fluid flow are obtained from the law of conservation of mass which is obtained from continuity equation (Equation (1)) and momentum (Equations (2)–(4)). These are in the form of partial differential equations.

FLOW-3D applies different numerical methods to solve equations of fluid motion, multi-physics, and multiscale problems to obtain solutions that are generally transient and 3 dimensional. The choice of FLOW-3D was based on the 3D nature of flows in most hydraulic structures in FLOW-3D, area and volume porosity are considered in all equations using the fractional area/volume obstacle representation (FAVOR) method. The FAVOR is a checking algorithm that checks the .stl files for geometric resolutions, it only shows how the solver will interpret the geometry.

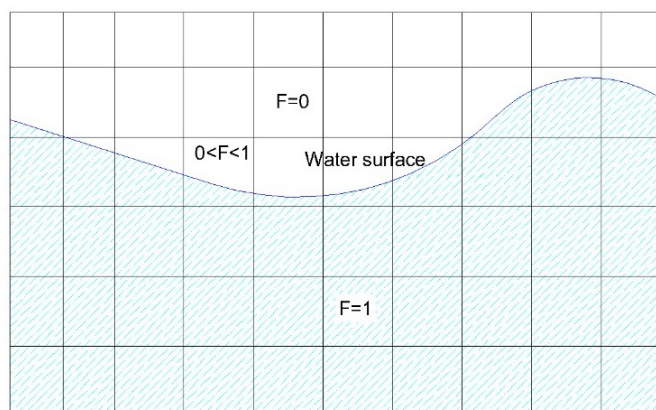


Figure 2. Water volume fraction representation.

For three dimensional incompressible flows, the governing equations utilized by FLOW-3D are as summarized in the Equations below [28]:

$$V_F \frac{\partial \rho}{\partial t} + \frac{\partial}{\partial x} (u A_x) + \frac{\partial}{\partial y} (v A_y) + \frac{\partial}{\partial z} (w A_z) = \frac{R_{SOR}}{\rho} \quad (1)$$

where V_F indicates the fraction of open volume to flow; ρ is the density, the velocity components, fractional areas in the x , y and z directions are u , v , w , A_x , A_y and A_z , and the source term of density is R_{SOR} .

$$\frac{\partial u}{\partial t} + \frac{1}{V_F} \left(u A_x \frac{\partial u}{\partial x} + v A_y \frac{\partial u}{\partial y} + w A_z \frac{\partial u}{\partial z} \right) = -\frac{1}{\rho} \frac{\partial p}{\partial x} + G_x + f_x \quad (2)$$

$$\frac{\partial v}{\partial t} + \frac{1}{V_F} \left(u A_x \frac{\partial v}{\partial x} + v A_y \frac{\partial v}{\partial y} + w A_z \frac{\partial v}{\partial z} \right) = -\frac{1}{\rho} \frac{\partial p}{\partial y} + G_y + f_y \quad (3)$$

$$\frac{\partial w}{\partial t} + \frac{1}{V_F} \left(u A_x \frac{\partial w}{\partial x} + v A_y \frac{\partial w}{\partial y} + w A_z \frac{\partial w}{\partial z} \right) = -\frac{1}{\rho} \frac{\partial p}{\partial z} + G_z + f_z \quad (4)$$

where p is pressure, G_x , G_y and G_z are body accelerations in the coordinate direction (x, y, z) and (f_x, f_y, f_z) are viscous accelerations in the coordinate direction (x, y, z) . The turbulence model used in this research paper is the RNG as it gives better performance when compared with other models [27]. The equations used are as in Equations (5) and (6) below:

$$\frac{\partial}{\partial t} (\rho k) + \frac{\partial}{\partial x_i} (\rho k u_i) = \frac{\partial}{\partial x_j} \left[\left(\mu + \frac{\mu_t}{\sigma_k} \right) \frac{\partial k}{\partial x_j} \right] + P_k - \rho \epsilon \quad (5)$$

$$\frac{\partial}{\partial t} (\rho \epsilon) + \frac{\partial}{\partial x_i} (\rho \epsilon u_i) = \frac{\partial}{\partial x_j} \left[\left(\mu + \frac{\mu_t}{\sigma_\epsilon} \right) \frac{\partial \epsilon}{\partial x_j} \right] + C_{1\epsilon} \frac{\epsilon}{k} P_k - C_{2\epsilon} \rho \frac{\epsilon^2}{k} \quad (6)$$

where ϵ is the energy dissipation rate per unit mass, k is the turbulent kinetic energy per unit mass (TKE), t is the time, x_i is the coordinate in the i -axis, μ is the dynamic viscosity, μ_t is the turbulent dynamic viscosity, and P_k is the production of TKE. The remaining terms $C_{1\epsilon} = 1.42$; $C_{2\epsilon} = 1.68$; $\sigma_k = \sigma_\epsilon = 1.39$ according to [27]. The turbulent viscosity is computed using the parameter $C_\mu = 0.085$ using Equation (7).

$$\mu_t = \rho C_\mu \frac{k^2}{\epsilon} \quad (7)$$

3. Numerical Simulation Setup

3.1. Geometry Creation and Model Setup

The simulations were carried out on a Core i7 3770 CPU and 3.40 GHz, 16 GB RAM Computer. The geometry of the REDAC module plates was created using SOLIDWORKS CAD software as shown in Figure 3 below. The design was simplified from a whole module box with dimension of 30 cm \times 30 cm \times 71 cm to a total of four plates for ease of meshing, reduction in computation time and because most of the noticeable changes occur in these plates. The geometry was then converted to stereolithography (STL) file format and imported into FLOW-3D. The solution was run on a steady-state watch list with total mass, the average mean kinetic energy, the average mean turbulent energy and the average mean turbulent dissipation activated. The interface tracking was a free surface or sharp interface with one fluid (incompressible), the simulations units were set to the centimeter–gram–second system of units (CGS). Also, in the physics of the system, the noninertial reference frames were specified and imputed. The fluid was set to viscous and RNG model was selected with no-slip as the wall shear boundary conditions in the viscosity and turbulence tab. In the material properties, water at 20 °C with all its properties like density and viscosity were uploaded as the fluid.

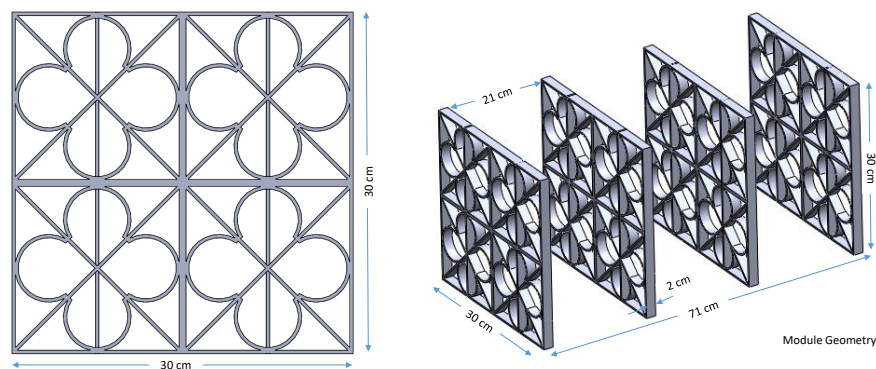


Figure 3. REDAC module geometry.

3.2. Meshing and Sensitivity Analysis

The meshing was done using non-conforming mesh blocks. The sensitivity analysis was done according to the results of the FAVOR and total mesh sizes as shown in Figure 4 which translates to computational time as highlighted by [21]. Table 1 summarizes the mesh sizes, total number of grids as well as the downstream velocity (DSV) variations. For this study, the mesh size of 0.21 cm was adopted because of the computation time, FAVOR results and values of the downstream velocity (DSV) obtained. In order to minimize the running time, half of the model was simulated as it is symmetrical.

Table 1. Mesh sensitivity analysis.

Test Number	Mesh Size	Total Grid (Millions)	DSV (cm/s)
1	0.26	1.78	45.30
2	0.21	3.41	46.50
3	0.17	6.41	48.60

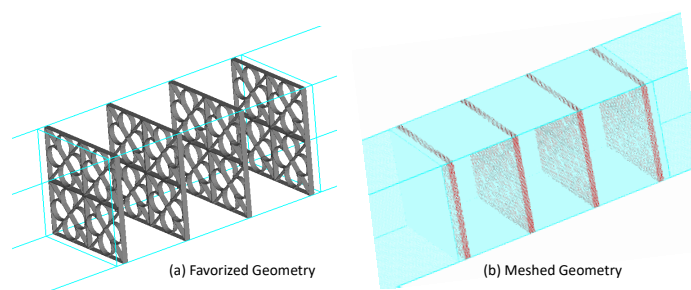


Figure 4. Favorized and meshed geometry.

3.3. Boundary Conditions and Solution Initialization

The inlet was set to velocity inlet (V) with a value of 38 cm/s and an initial fluid elevation of 8.3 cm (y), while y_1 is the downstream water depth. Also, the top was set to atmospheric pressure with fluid fraction (α) = 0. While the right and bottom sides were set to wall (W). Also, the left side was set to symmetry (S) because the geometry was considered symmetry, therefore to save computation time, half of it was simulated. The outlet was set to pressure outlet (P) with a fluid elevation of 2 cm as shown in Figure 5. The fluid was initialized with hydrostatic pressure at the global case and a velocity of 38 cm/s was specified at the fluid region. The water depth of 8.3 cm was specified in the y limiters. Two history probes and fluxes were specified at a distance of 40 cm before the module upstream and 40 cm after the module at downstream to monitor hydraulic parameter variations with time. At the output stage, the fluid fraction, fluid velocities, hydraulic data (including depth-averaged values, maximum flow depth, Froude's number, specific hydraulic head, and total hydraulic head) were selected. Nothing was changed at the numeric stage.

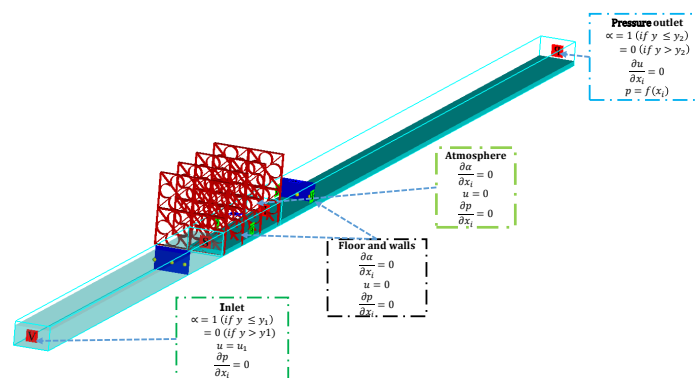


Figure 5. Boundary conditions.

4. Design of the Validation Experiments in the Laboratory

To verify the accuracy and credibility of the numerical simulation method adopted in this study, a simplified experiment was carried out in the laboratory. The full scale of the experiments were carried out at the hydraulic laboratory of REDAC, Universiti Sains Malaysia (USM) and the single module experiments were conducted at the hydraulic laboratory of Universiti Teknologi Petronas (UTP). For the purpose of this study, the validation was done with the results from UTP laboratory. The experiments involved using a 10 m length, 0.3 m width and 0.6 m high re-circulating flume made from glass as shown in Figure 6. Also, the testing points in the experiments are highlighted in Figure 7.

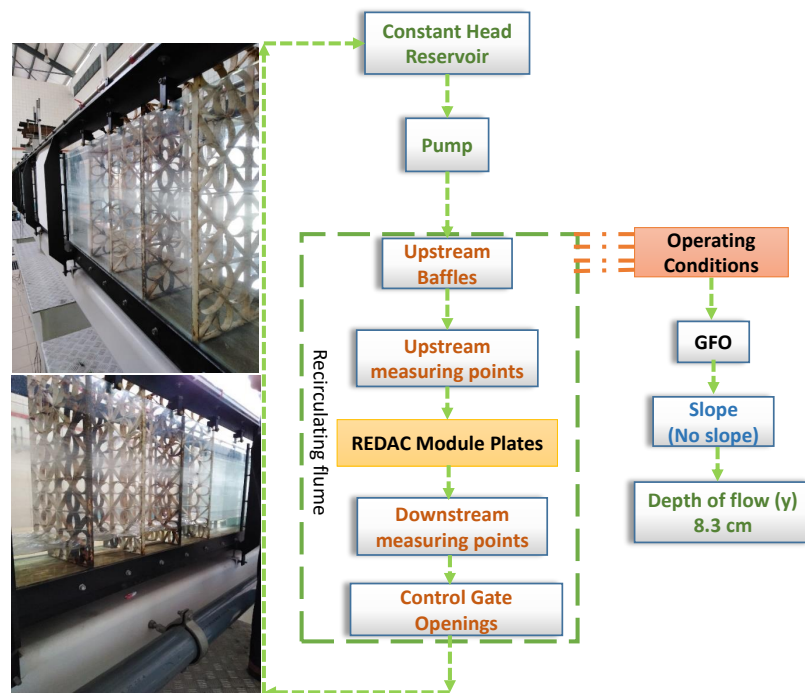


Figure 6. Operating conditions and module setup.

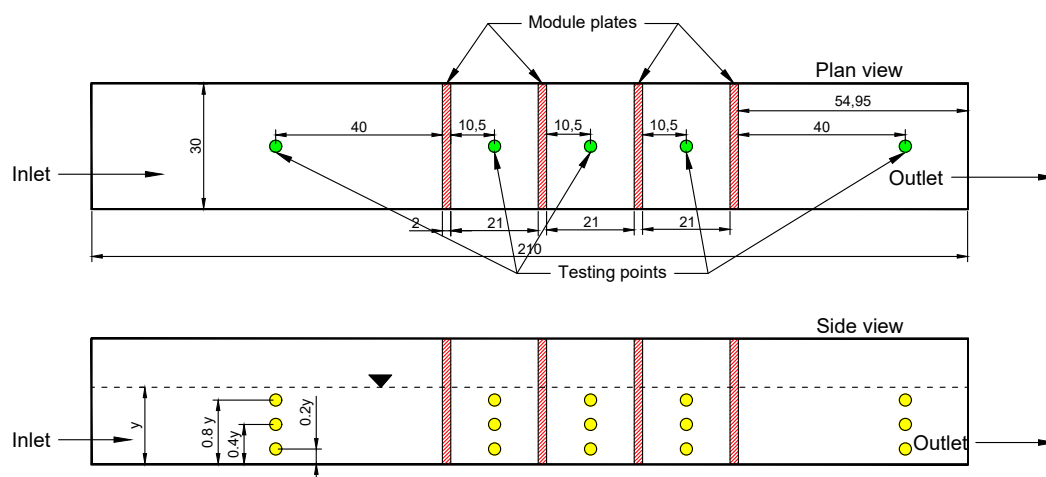


Figure 7. Testing points in the experiments.

The Laboratory equipment used include a flow meter, four (4) REDAC module plates, re-circulating flume and a piece of point gauge as shown in Figure 8. During the experiments, a single pump was used to supply water to the flume through a pipe connected to the storage tanks beneath the flume. Some baffles were installed at the upstream to regulate the turbulence effects at the

inlet point. At the start of the experiments, the flat gate located at the outlet point downstream was opened. Two stages were considered during the experiments including FFWM (for control purpose) and FWM to understand the effects of the module. The target parameters during the experiments were velocity variation and water surface profile.

From fully defined geometry, a simplified geometry that represents the most relevant characteristics of the module, ease computation time and cost was developed [17]. To coincide with the numerical simulations and for ease of validation, the same depth of 8.3 cm was used in the flume during the experiment. The setup consisted of a complete REDAC module box with the same dimensions as in the numerical simulation. The test locations are at the centre of the channel with various depths as highlighted in Figure 7 with hydraulic gate fully opened (GFO) at the downstream. During each experiment, measurements were taken after 10 minutes when the flow became steady and fully developed.



Figure 8. Laboratory setup and equipments.

The current meter records the number of rotations (p) for 30 s. The number of propeller rotations per second (N) was calculated using $N = p/30$ and then the velocity (m/s) was calculated by using Equations (8) and (9) depending on the values of N .

$$v = 0.0123 + 0.2473 * N, 0.00 < N < 1.74 \quad (8)$$

$$v = -0.0042 + 0.2568 * N, 1.74 < N < 10 \quad (9)$$

4.1. Estimation of Manning's Coefficient

The amount of resistance on flow in open channels is determined by Manning's roughness coefficient. A decrease in flow means higher roughness coefficient according to [29]. For the purpose of this study, the roughness coefficient was calculated using Equation (10).

$$v = \frac{R^{2/3} \sqrt{S_0}}{n} \quad (10)$$

where v , R , S_0 , and n are the velocity in cm/s, hydraulic radius cm, slope and Manning's roughness coefficient respectively.

4.2. Froude and Reynold's Number (Fr , Re)

Froude's number (Fr) represents the ratio of inertial to gravity forces. Mathematically, it is defined in Equation (11).

$$Fr = \frac{v}{\sqrt{gY}} \quad (11)$$

where v , Y and g represent the velocity, flow depth and acceleration due to gravity.

The Reynold's number was calculated from the Equation (12) below:

$$Re = \frac{vl}{\theta} \quad (12)$$

where v = average velocity (m/s) and l = characteristic length (m) and θ is the kinematic viscosity in m^2/s .

5. Results and Discussions

The numerical results were validated with the experimental in both FFWM and FWM. The model was then used to predict the variation of flow profile and provide clear visualization contour plots of flow patterns and the effect of the module on the water flow in terms of parameters such as velocity and Froude's number. Manning's roughness coefficients were also estimated for both cases numerically and compared with the experimental.

5.1. Numerical Model Validation

In order to ensure the validity and accuracy of the used FLOW-3D modelling software, it was verified with the experimental results for better prediction of flow pattern and other hydraulic features in the module. This was achieved by measuring velocities at two points before and after the module. The two points were at 40 cm at upstream (US) and downstream (DS) of the module as highlighted in Figure 7. The y -axis location was at the center ($y = 15$ cm) and the depth was located at a point $0.4d$ where d is the depth of the water from the channel bottom. The specific values obtained for probes 1 and 2 were as highlighted in Table 2. From the table, the experimental results were found to strongly agree with the numerical values with percentage error less than 5% in both parameters as highlighted, which is acceptable according to [30]. The difference may be due to mesh quality variation from the numerical results.

Table 2. Validation of numerical with experimental results.

Flow Parameter		Working Conditions					
		FFWM			FWM		
		Exp.	Num.	% Error	Exp.	Num.	% Error
Flow Velocity (cm/s)	US	51.6	50.40	2.38	42.00	43.50	3.45
	DS	52.5	53.18	1.28	44.50	46.50	4.30
Flow Depth (cm)	US	7.6	7.71	1.43	7.65	7.75	1.29
	DS	6.38	6.52	2.15	6.30	6.50	3.08

Furthermore, after stabilization conditions were reached in the FWM case, the variation of flow profiles in both the experimental and numerical were also plotted (at $y = 15$ cm or center of the flume) as in Figure 9. Herein, a reasonable correlation can be observed clearly as the flow moves from upstream through the module plates to the downstream. The effects of the module can clearly be visualized with a clear variation of the average flow depth from about 7.75 cm to nearly 6.50 cm with less than 5% error between the numerical and experimental values. Accordingly, an increase in the flow velocity and Froude's number from 43.50 cm/s to about 46.50 cm/s and 0.50 to about 0.59, respectively, can be

observed as shown in Figure 10a,b. This is clear evidence that the module alters the flow pattern and create the needed delay of the flow from reaching the downstream faster.

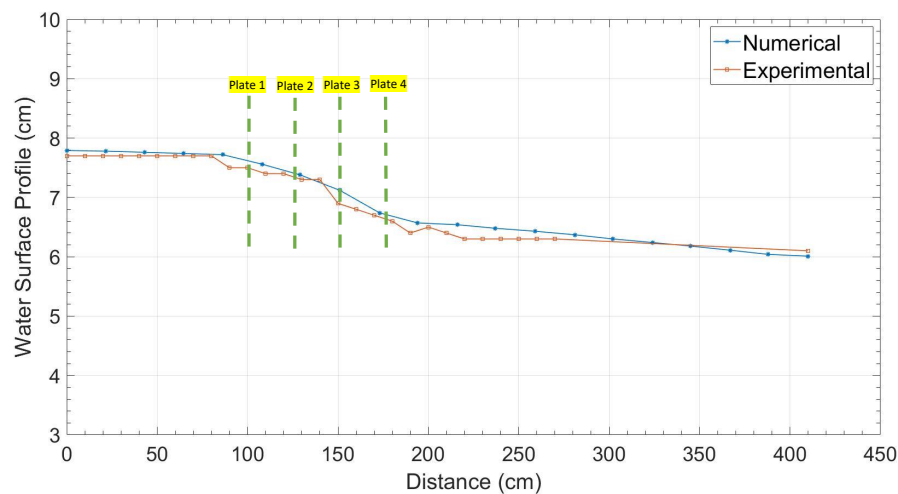


Figure 9. Water surface profile validation of FWM.

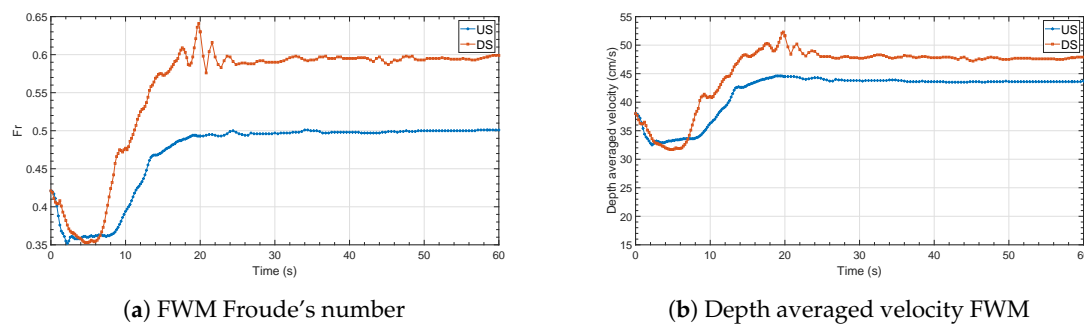


Figure 10. Flow depth, velocity and Fr variations in FWM.

5.2. Free Flow without Module and Flow with Module

As the flow becomes fully developed without and with single module installed in the flume, Figure 11 shows the volume flow rate (VFR) variations from the inlet to the outlet at the two fluxes specified with flux 1 at 40 cm before the module at US and flux 2 at 40 cm after the module at the DS. From the two graphs, it can be seen clearly that the mass conservation equation was obeyed with the inflow almost equal to the outflow both coinciding at $4750 \text{ cm}^3/\text{s}$ ($0.00475 \text{ m}^3/\text{s}$) in both the FFWM and FWM.

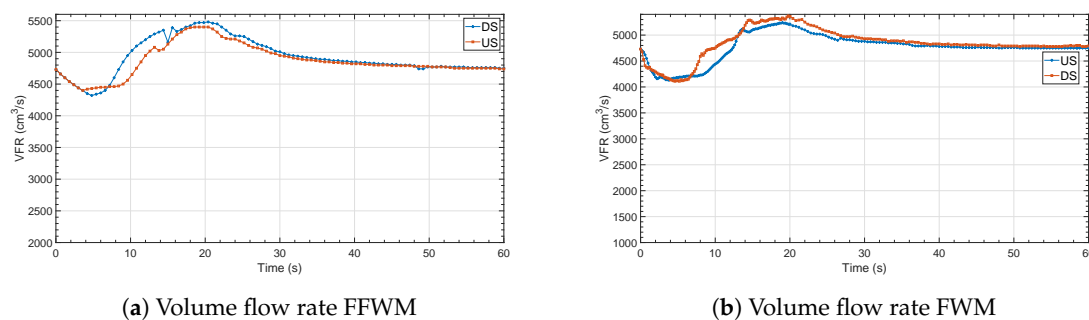


Figure 11. VFR comparison of FWM and FFWM.

The FFWM was for control purpose to ascertain the effects of the module on the flow path. After stabilization of the flow, parameters such as the depth-averaged flow velocity and Froude's number in both the two cases as shown in Figures 12 and 13. From the Figures, it can be observed clearly in the velocity distribution of the FFWM that the velocity increases uniformly from the upstream to the downstream with a maximum of about 60 cm/s at the surface. In the same case, the Froude's number varies to a highest of about 0.7 (subcritical, $Fr < 1$) at the surface. On the other hand, the flow can be observed to be highly turbulent ($Re > 4000$) due to the presence of the module plates with the velocity distribution not uniformly distributed. The velocity can be observed to increase as the flow moves across the plates with the highest at the downstream location 3 as in Figure 13. Also, stagnation points (zones of higher pressure and lower velocities) are noticed at locations 2 and the velocities were minimum at the location of the wall 1. In addition, the velocities were observed to increase across the perforations and are less at the plates. The flow later stabilizes after the module and moved downstream. The effects of the module on the flow pattern can clearly be observed in reducing the velocity and increasing the pressure thereby creating the needed delay in the flow from reaching the outlet faster.

Similarly, the Froude's number in the FWM case can be observed to behave increase a little due to the effect of the single module and the effects of the module pattern can be observed in the highlighted locations 1, 2 and 3 in the Figure 13 with the highest Fr at the center of the module perforations (with a maximum value of about 0.85) within location 3. The flow in both cases can be considered to be subcritical in nature ($Fr < 1$). This is due to the fact that the whole length of the flume was simulated with the single module inside which in real sense will have less effect compared to when a larger number of modules are used and the fact that the experiments and numerical simulations were all carried out without the effect of the slope.

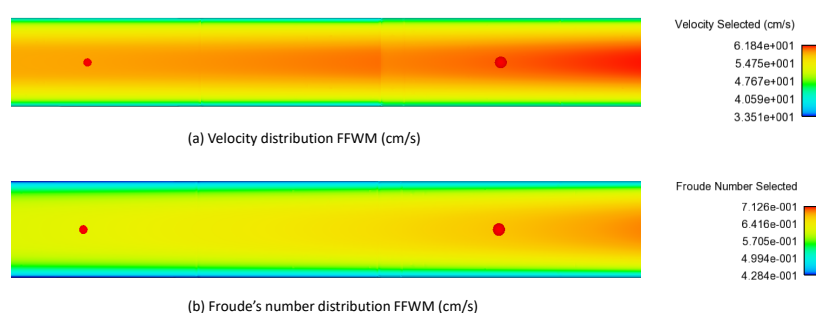


Figure 12. Contour plot of velocity and Fr of FFWM.

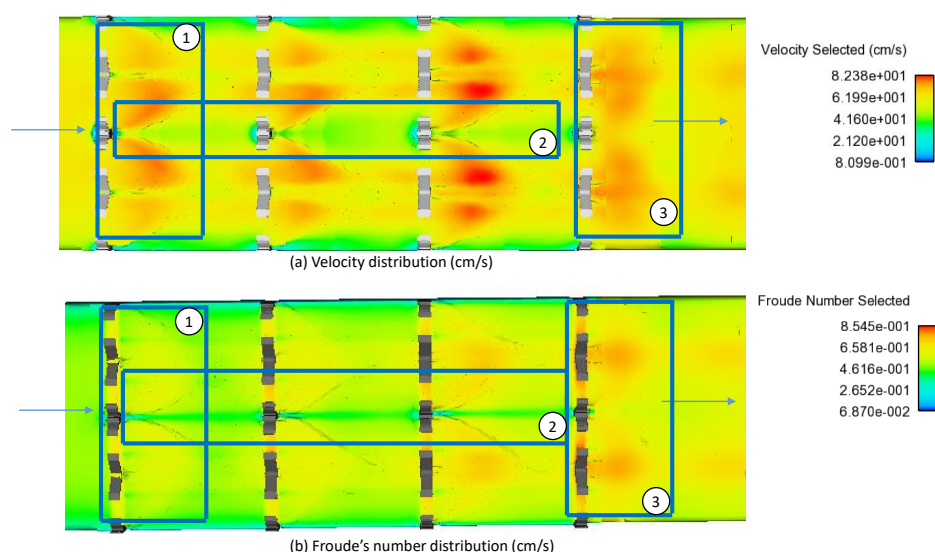


Figure 13. Contour plot of velocity and Fr of FWM.

5.3. Effects of the Module on Manning's Roughness

Table 3 shows the summary of hydraulic parameters measured during the experiment and compared with numerical simulation results in FFWM as well as FWM cases. From the table, the roughness coefficients can be observed to agree very well in the FFWM case for both probing points in the numerical and experimental results with minor variations. Also, a slight increase in the Manning's roughness value at the upstream in the case of FWM when compared with the case of FFWM can be observed due to the presence of the module in the channel. This increase, however, was evidence of flow resistance in the channel as Manning's roughness coefficient represents a measure of the amount of frictional resistance to flows when passing through channel features [29]. The slightly higher values in the Manning's roughness can be attributed to the fact that the simulation and the experiments were carried on flatbeds with no slope and also the fact that the whole flume length of 10 m was tested in the experiment and simulated with the single module installed. These findings are in agreement with the work of Choo et al. [31] and Cheng et al. [32] who observed Manning's coefficient variations under greater flow depth.

Table 3. Hydraulic parameters for FWM and FFWM.

Case			Flow Depth (cm)	Average Vel (cm/s)	Wetted Perimeter (cm)	Hydraulic Radius (cm)	Manning's Roughness (s/cm ^{1/3})
FFWM	Experimental	US	7.60	51.60	45.20	5.04	0.06
		DS	6.38	52.50	42.76	4.48	0.05
	Numerical	US	7.71	50.40	45.42	5.09	0.06
		DS	6.52	53.18	43.14	4.54	0.05
FWM	Experimental	US	7.65	42.00	45.30	5.07	0.07
		DS	6.30	44.50	42.60	4.44	0.06
	Numerical	US	7.75	43.50	45.50	5.11	0.07
		DS	6.50	46.50	43.00	4.53	0.06

5.4. Contour Plots of Velocity and Flow Pattern Visualization

For clear visualization of the effects of the module pattern on the flow parameters, Figure 14 shows the 2D contour plots of velocity variations along the lateral directions from sides at (a) $y = 2$ cm and (c) $y = 15$ cm and center of the perforation (c) $y = 7.5$ cm of the module from the positive y -axis. From the Figure, it can clearly be seen that the velocity decrease at the sides with (a) in the range of 17–34 cm/s, and (c) in the range of 34 cm/s to 51 cm/s with highest points located at the outlets. The lower velocity range can be ascribed to the area of stagnation mostly as a result of the module pattern that blocks the flow. The highest velocity can be observed in (b) as a result of free flow with no stagnation from the module pattern, the velocity is in the range of 34–68 cm/s and can also be observed highest at the outlet. These values signify the impact of the module plates on the flow velocity and can generally be observed that the higher the perforation, the higher the velocity of flow in the flume. These effects can be translated to an increase in resistance of flow at the upstream and a delay in the flow from reaching the outlet immediately which is the main goal of the subsurface module.

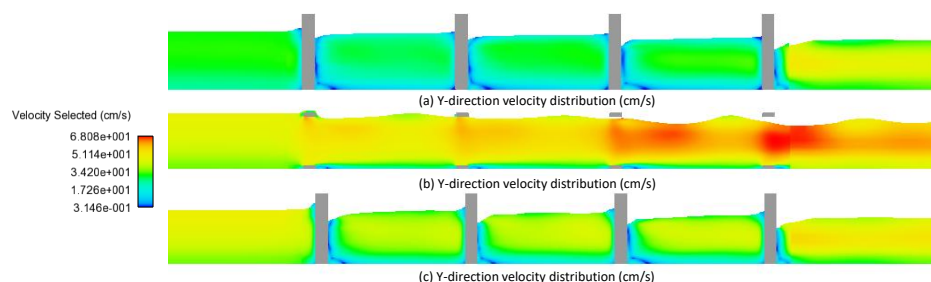


Figure 14. 2D plots of velocity contours along lateral distance.

Additionally, Figure 15 shows the flow pattern, turbulence effects as well as the velocity variations in 3D across the module plates. From the Figure, it can be clearly seen that the velocity is increasing as the flow passes from one plate to another and along the lateral direction. This increase can be ascribed directly to the effect of the module pattern on the flow. The velocity is clearly high at the downstream compared to the upstream.

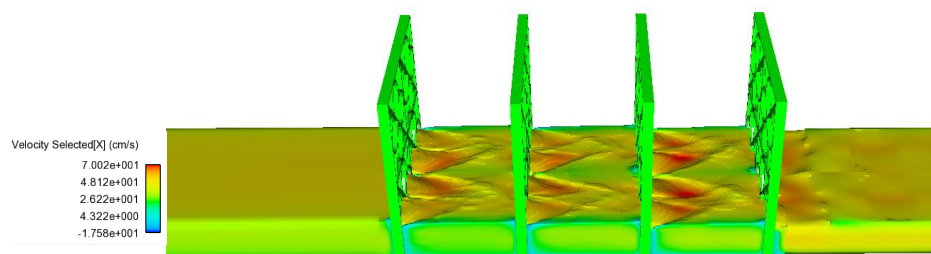


Figure 15. 3D plots of velocity isosurface along lateral distance.

6. Conclusions

In this study, the hydrodynamics of flows in the REDAC module was assessed and analyzed using both numerical and experimental techniques under two cases of FFWM and FWM. From the results and discussions, the following conclusions can be drawn:

REDAC module was able to alter the pattern and creates flow resistance by increasing the pressure at the upstream, depth-averaged flow velocity (43.50 to about 46.50 cm/s) at the downstream and decreasing water depth (7.75–6.50 cm). These variations can be attributed to the complex nature of the module pattern with more increase across the porous openings.

The CFD software used (FLOW-3D) was able to model the module behavior with greater certainty. This is because it was able to visualize the flows in 2D and 3D showing clear variations of target parameters and the fact that numerical results strongly agree with the experimental values with percentage errors less than 5%. This means that certain laboratory detailed parameters and visualizations can be studied with a high degree of confidence and accuracy with this model. Therefore, this technique can be used to characterize the behavior of fluid in larger arrangements of modules and under different flow conditions without the need for expensive laboratory experiments such as in BIOECODS swale system.

Author Contributions: Conceptualization A.S.A.; K.W.Y.; H.T.; and A.A.G. Methodology A.S.A.; Software, A.S.A.; A.A.G. and E.H.H.A.; Validation A.S.A.; Formal analysis, A.S.A.; E.H.H.A.; Investigation, A.S.A.; Resources, A.S.A.; K.W.Y.; Data curation, A.S.A.; M.K.Z.; E.H.H.A.; Writing original draft preparation, A.S.A.; E.H.H.A.; Writing review and editing, A.S.A.; K.W.Y.; H.T.; A.A.G.; M.K.Z.; E.H.H.A.; M.M.M.; A.T.S.; M.O.; M.S.P.; Supervision, K.W.Y.; H.T.; A.A.G.; Funding acquisition, K.W.Y.

Funding: This research was funded by the Fundamental Research Grant Scheme (FRGS) of Ministry of Higher Education Malaysia (MOHE) with grant number: 015MA0-034.

Acknowledgments: The authors acknowledge Universiti Teknologi PETRONAS, Malaysia, River Engineering and Urban Drainage Research Centre (REDAC), Universiti Sains Malaysia for providing the enabling environment and hydraulic laboratories to be utilized for this research. The research was funded by Fundamental Research Grant Scheme (FRGS) of Ministry of Higher Education Malaysia (MOHE) with grant number: 015MA0-034.

Conflicts of Interest: The authors declare no conflict of interest.

Abbreviations

The following abbreviations are used in this manuscript:

BIOECODS	Bio-Ecological Drainage System
REDAC	River Engineering and Urban Drainage Research Centre
DID	Department of Irrigation and Drainage
FWM	Flow With Module
FFWM	Free Flow Without model
CFD	Computational Fluid Dynamics
VOF	Volume Of Fluid
FAVOR	Fractional Area/Volume Obstacle Representation
RNG	Re-Normalisation Group
STL	Stereolithography
CGS	Centimetre–Gram–Second system
MB	Mesh Block
DS	Downstream
US	Upstream
DSV	Downstream Velocity
GFO	Gate Fully Opened
USM	Universiti Sains Malaysia
Num	Numerical
Exp	Experimental
Vel	Velocity

Nomenclature

The following nomenclature are used in this manuscript:

V_F	fluid volume function
p	pressure
G_x	Body acceleration in x coordinate
G_y	Body acceleration in y coordinate
G_z	Body acceleration in z coordinate
ϵ	Energy dissipation rate
k	Turbulence kinetic energy
t	Time (s)
x_i	Coordinate in the i axis
μ	Dynamic viscosity
μ_t	Turbulent dynamic viscosity
P_k	Production of TKE
v	Velocity (cm/s)
f_x	Viscous accelerations in the x direction
f_y	Viscous accelerations in the y direction
f_z	Viscous accelerations in the z direction

References

1. Abdurraheed, A.S.I.; Yusof, K.W.; Takaijudin, H.B.; Ghani, A.A.; Muhammad, M.M.; Sholagberu, A.T. Advances and Challenging Issues in Subsurface Drainage Module Technology and BIOECODS: A Review. In Proceedings of the International Conference on Civil, Offshore & Environmental Engineering (ICCOEE2018), Kuala Lumpur, Malaysia, 13–15 August 2018; Volume 203, p. 07005.
2. Abdurraheed, A.S.I.; Yusof, K.W.; Takaijudin, H.B.; Ab, A.; Iskandar, B.S. Effects of backwater on hydraulic performance evaluation of rainsmart modules in sustainable drainage systems. In Proceedings of the International Conference on Water Resources, Langkawi, Malaysia, 27–28 November 2018.
3. Ainan, A.; Zakaria, N.A.; Ghani, A.A.; Abdullah, R.; Sidek, L.M.; Yusof, M.F.; Wong, L.P. Peak flow attenuation using ecological swale and dry pond. *Adv. Hydro-Sci. Eng.* **2003**, *6*, 1–9.
4. Barber, M.E.; King, S.G.; Yonge, D.R.; Hathhorn, W.E. Ecology ditch: A best management practice for storm water runoff mitigation. *J. Hydrol. Eng.* **2003**, *8*, 111–122.

5. Fletcher, T.D.; Shuster, W.; Hunt, W.F.; Ashley, R.; Butler, D.; Arthur, S.; Mikkelsen, P.S. SUDS, LID, BMPs, WSUD and more—The evolution and application of terminology surrounding urban drainage. *Urban Water J.* **2015**, *12*, 525–542.
6. Hammond, M.J.; Chen, A.S.; Djordjević, S.; Butler, D.; Mark, O. Urban flood impact assessment: A state-of-the-art review. *Urban Water J.* **2015**, *12*, 14–29.
7. Zakaria, N.A.; Ab Ghani, A.; Abdullah, R.; Mohd. Sidek, L.; Ainan, A. Bio-ecological drainage system (BIOECODS) for water quantity and quality control. *Int. J. River Basin Manag.* **2003**, *1*, 237–251.
8. Benisi Ghadim, H.; Sai Hin, L.; Hooi Bu, C.; Jie Chin, R. Effectiveness of BIOECODS for peak flow attenuation: an appraisal using InfoWorks SD. *Hydrol. Sci. J.* **2017**, *62*, 421–430.
9. Muhammad, M.M.; Yusof, K.W.; Mustafa, M.R.; Ghani, A.A. Hydraulic assessment of grassed swale as bioengineered channel. In *Engineering Challenges for Sustainable Future*; ROUTLEDGE in Association with GSE Research, Kuala Lumpur, Malaysia: 2016; Volume 273, pp. 273–278.
10. Ahmad, N.A.; Ghani, A.A.; Zakaria, N.A. Hydraulic Characteristic for Flow in Swales. 2011. Available online: http://redac.eng.usm.my/html/publish/2011_23.pdf (accessed on 25 July 2019)
11. Lai, S.H.; Kee, L.C.; Zakaria, N.A.; Ghani, A.A.; Chang, C.K.; Leow, C.S. Flow Pattern and Hydraulic Characteristic for Subsurface Drainage Module. In Proceedings of the International Conference on Water Resources (ICWR 2009), Kedah, Malaysia, 26–27 May 2009.
12. Muhammad, M.M.; Yusof, K.W.; Mustafa, M.R.U.; Zakaria, N.A.; Ghani, A.A. Artificial neural network application for predicting drag coefficient in flexible vegetated channels. *J. Telecommun. Electron. Comput. Eng. (JTEC)* **2018**, *10*, 99–102.
13. Zakaria, N.A.; Takara, K.; Abdullah, R.; Sidek, L.M.; Ghani, A.A. *Bio-Ecological Drainage Systems (Bioecods): An Integrated Approach for Urban Water Environmental Planning*; International Islamic University Malaysia, Kuala Lumpur, Malaysia: 2004.
14. Kee, L.C.; Zakaria, N.A.; Lau, T.L.; Chang, C.K.; Ghani, A.A. Determination of Manning's n for Subsurface Modular Channel. 2011. Available online: http://redac.eng.usm.my/html/publish/2011_25.pdf (accessed on 25 July 2019).
15. Muhammad, M., Yusof, K., Mustafa, M.; Zakaria, N.; Ghani, A.A. Hydraulic performance of sub-surface drainage module. In Proceedings of the IAHR World Congress, Kuala Lumpur, Malaysia, 13–18 August 2017; pp. 6059–6066.
16. Pradhan, A.; Khatua, K.K. Assessment of roughness coefficient for meandering compound channels. *KSCE J. Civ. Eng.* **2017**, *22*, 2010–2022.
17. Sánchez-Beltrán, H.; Rodríguez, C.M.; Triviño, J.B.; Iglesias-Rey, P.L.; Valderrama, J.S.; Martínez-Solano, F.J. Characterization of modular deposits for urban drainage networks using CFD techniques. *Procedia Eng.* **2017**, *186*, 84–92.
18. Faram, M.G.; Guymer, I.; Saul, A.J. Assessment of modular block stormwater storage systems. In Proceedings of the NOVATECH: 5th International Conference on Sustainable Techniques and Strategies in Urban Water Management, Lyon, France, 6–10 June 2004; pp. 235–242.
19. Jarman, D.S.; Faram, M.G.; Butler, D.; Tabor, G.; Stovin, V.R.; Burt, D.; Throp, E. Computational Fluid Dynamics as a Tool for Urban Drainage System Analysis: A Review of Applications and Best Practice. 2008. Available online: <http://hdl.handle.net/10036/4259> (accessed on 25 July 2019).
20. Savage, B.M.; Crookston, B.M.; Paxson, G.S. Physical and numerical modeling of large headwater ratios for a 15 labyrinth spillway. *J. Hydraul. Eng.* **2016**, *142*, 04016046.
21. Choufu, L.; Abbasi, S.; Pourshahbaz, H.; Taghvaei, P.; Tfwala, S. Investigation of Flow, Erosion, and Sedimentation Pattern around Varied Groynes under Different Hydraulic and Geometric Conditions: A Numerical Study. *Water* **2019**, *11*, 235.
22. Lo, D.C.; Liou, J.S.; Chang, S. Hydrodynamic performances of air-water flows in gullies with and without swirl generation vanes for drainage systems of buildings. *Water* **2015**, *7*, 679–696.
23. Hirt, C.W.; Nichols, B.D. Volume of fluid (VOF) method for the dynamics of free boundaries. *J. Comput. Phys.* **1981**, *39*, 201–225.
24. Sousa, J.P.M.; Moya, R.A.C.; Prohasky, D.; Vaz, C.E.V. Empirical analysis of three wind simulation tools to support urban planning in early stages of design. *Blucher Des. Proc.* **2015**, *2*, 363–370.
25. Li, G.; Li, X.; Ning, J.; Deng, Y. Numerical Simulation and Engineering Application of a Dovetail-Shaped Bucket. *Water* **2019**, *11*, 242.

26. Jarman, D.S.; Faram, M.G.; Tabor, G.; Butler, D. A review of the opportunities presented through the application of Computational Fluid Dynamics (CFD) to water management challenges. In Proceedings of the Water Management Challenges in Global Change, CCWI2007 and SUWM2007 Conference, Leicester, UK, 3–5 September 2007.
27. Bayon, A.; Valero, D.; García-Bartual, R.; López-Jiménez, P.A. Performance assessment of OpenFOAM and FLOW-3D in the numerical modeling of a low Reynolds number hydraulic jump. *Environ. Model. Softw.* **2016**, *80*, 322–335.
28. Kim, S.D.; Lee, H.J.; An, S.D. Improvement of hydraulic stability for spillway using CFD model. *Int. J. Phys. Sci.* **2010**, *5*, 774–780.
29. Mustafa, N.; Ahmad, N.A.; Razi, M.A.M. Variations of roughness coefficients with flow depth of grassed swale. In *IOP Conference Series: Materials Science and Engineering*; IOP Publishing: Bristol, UK, 2016; p. 012082.
30. Zahabi, H.; Torabi, M.; Alamatian, E.; Bahiraei, M.; Goodarzi, M. Effects of Geometry and Hydraulic Characteristics of Shallow Reservoirs on Sediment Entrapment. *Water* **2018**, *10*, 1725.
31. Choo, K.L. Determination of Flow Resistance in Modular Open Channel. Master's Thesis, River Engineering and Urban Drainage Research Centre REDAC, Parit Buntar, Malaysia, 2011.
32. Chen, Y.C.; Kao, S.P.; Lin, J.Y.; Yang, H.C. Retardance coefficient of vegetated channels estimated by the Froude number. *Ecol. Eng.* **2009**, *35*, 1027–1035.



© 2019 by the authors. Licensee MDPI, Basel, Switzerland. This article is an open access article distributed under the terms and conditions of the Creative Commons Attribution (CC BY) license (<http://creativecommons.org/licenses/by/4.0/>).